Cell Reports

NMDAR-Dependent Emergence of Behavioral Representation in Primary Visual Cortex

Graphical Abstract

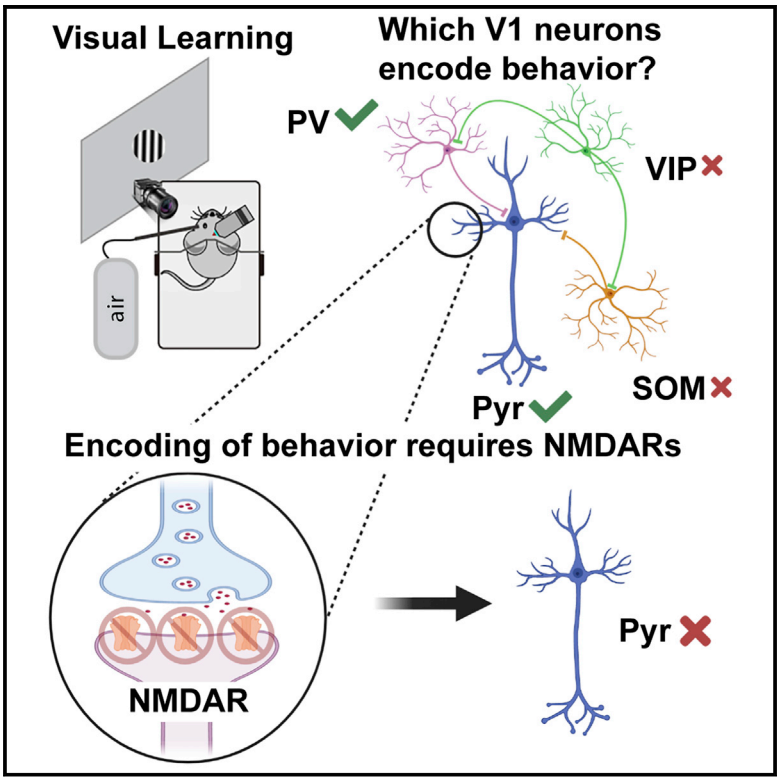

Highlights

- V1 pyramidal cells show experience-dependent emergence of behavioral representation
- Behavior is also encoded by PV- but not SOM- or VIP-expressing interneurons
- Emergent behavioral prediction requires cell-autonomous NMDAR expression

Authors

Alicja Puścian, Hadas Benisty, Michael J. Higley

Correspondence

m.higley@yale.edu (M.J.H.), a.puscian@nencki.edu.pl (A.P.), hadas.benesti@yale.edu (H.B.)

In Brief

Puścian et al. show that pyramidal and parvalbumin-expressing neurons in mouse visual cortex predict single-trial performance on a visual detection task. Prediction accuracy emerges with learning, is not observed for somatostatin- or vasoactive intestinal peptide-expressing cells, and requires cell-autonomous NMDA receptor (NMDAR) expression. These results highlight plasticity of behavioral representations in the primary sensory cortex.

Puścian et al., 2020, Cell Reports *32*, 107970
July 28, 2020
https://doi.org/10.1016/j.celrep.2020.107970

Cell Reports

CellPress
OPEN ACCESS

Report

NMDAR-Dependent Emergence of Behavioral Representation in Primary Visual Cortex

Alicja Puścian,[1,2,*] Hadas Benisty,[1,*] and Michael J. Higley[1,3,*]
[1]Department of Neuroscience, Kavli Institute of Neuroscience, Yale University School of Medicine, New Haven, CT 06510, USA
[2]Nencki-EMBL Partnership for Neural Plasticity and Brain Disorders – BRAINCITY, Nencki Institute of Experimental Biology, Polish Academy of Sciences, Pasteur 3 Street, 02-093 Warsaw, Poland
[3]Lead Contact
*Correspondence: m.higley@yale.edu (M.J.H.), a.puscian@nencki.edu.pl (A.P.), hadas.benesti@yale.edu (H.B.)
https://doi.org/10.1016/j.celrep.2020.107970

SUMMARY

Although neocortical sensory areas are generally thought to faithfully represent external stimuli, cortical networks exhibit considerable functional plasticity, allowing them to modify their output to reflect ongoing behavioral demands. We apply longitudinal 2-photon imaging of activity in the primary visual cortex (V1) of mice learning a conditioned eyeblink task to investigate the dynamic representations of task-relevant information. We find that, although all V1 neurons robustly and stably encode visual input, pyramidal cells and parvalbumin-expressing interneurons exhibit experience-dependent emergence of accurate behavioral representations during learning. The functional plasticity driving performance-predictive activity requires cell-autonomous expression of NMDA-type glutamate receptors. Our findings demonstrate that accurate encoding of behavioral output is not inherent to V1 but develops during learning to support visual task performance.

INTRODUCTION

Primary sensory areas of the mammalian neocortex, including the primary visual cortex (V1), have traditionally been thought to faithfully represent features of external stimuli. However, the cortical representation of external stimuli is highly plastic over a range of temporal scales. For example, learning associations between sensory stimuli and behaviorally relevant outcomes drive alterations in neuronal structure, activity patterns, and perceptual ability (Frenkel et al., 2006; Gavornik and Bear, 2014; Goltstein et al., 2013; Jurjut et al., 2017; Li et al., 2019; Makino and Komiyama, 2015; Poort et al., 2015; Schoups et al., 2001; Wang et al., 2016; Yan et al., 2014; Yang and Maunsell, 2004). Furthermore, repeated pairing of a visual stimulus with a reward results in modification of feature selectivity (e.g., orientation preference) by single neurons in the primary visual cortex (V1) (Frenkel et al., 2006; Gavornik and Bear, 2014; Goltstein et al., 2013; Jurjut et al., 2017; Poort et al., 2015; Schoups et al., 2001; Yan et al., 2014; Yang and Maunsell, 2004). Neuronal activity corresponding to behavioral choice or trial outcome has also been described in the sensory cortex (Blake et al., 2006; Kwon et al., 2016; Poort et al., 2015; Ress and Heeger, 2003; Rutkowski and Weinberger, 2005; Shuler and Bear, 2006; Tang and Higley, 2020; Wiest et al., 2010). However, it is unclear whether the representation of behavioral output is inherent to V1, like feature selectivity, or instead, emerges dynamically during learning. Moreover, the cellular mechanisms underlying the functional reorganization of network activity are poorly understood.

Several groups have shown that classical eyeblink conditioning provides an excellent model for investigating the neural correlates of sensorimotor learning (Albergaria et al., 2018; Freeman and Steinmetz, 2011; Heiney et al., 2014; Siegel et al., 2015). We recently showed that mice rapidly learn to form associations between visual stimuli and aversive corneal air-puffs, resulting in expression of a conditioned blink response (Tang and Higley, 2020). Neuronal activity within V1 is required for task performance and significantly predicts behavioral outcome in expert animals (Tang and Higley, 2020). Here, we combined chronic *in vivo* two-photon imaging and genetic manipulation of targeted excitatory and inhibitory neuronal populations within mouse V1 to investigate the dynamics and cellular mechanisms linked to plasticity of sensory and behavioral representations during conditioning. Our results demonstrate that V1 neurons robustly and stably encode visual input throughout learning, regardless of the gradual reduction in the magnitude of stimulus-evoked activity. In contrast, representation of behavioral outcome emerges over the course of learning for both single neurons and neuronal ensembles. Notably, behavioral encoding was observed for both pyramidal neurons (PNs) and parvalbumin-expressing interneurons (PV-INs) but not for somatostatin (SOM)-expressing interneurons (INs) or vasoactive intestinal peptide (VIP)-expressing INs. Finally, plasticity of behavioral representation requires cell-autonomous expression of NMDA-type glutamate receptors (NMDARs), suggesting a critical role for synaptic plasticity in the emergence of task-relevant activity in V1.

RESULTS

To study the relationship between V1 activity and the acquisition of sensory-guided behavior, we developed a visually cued

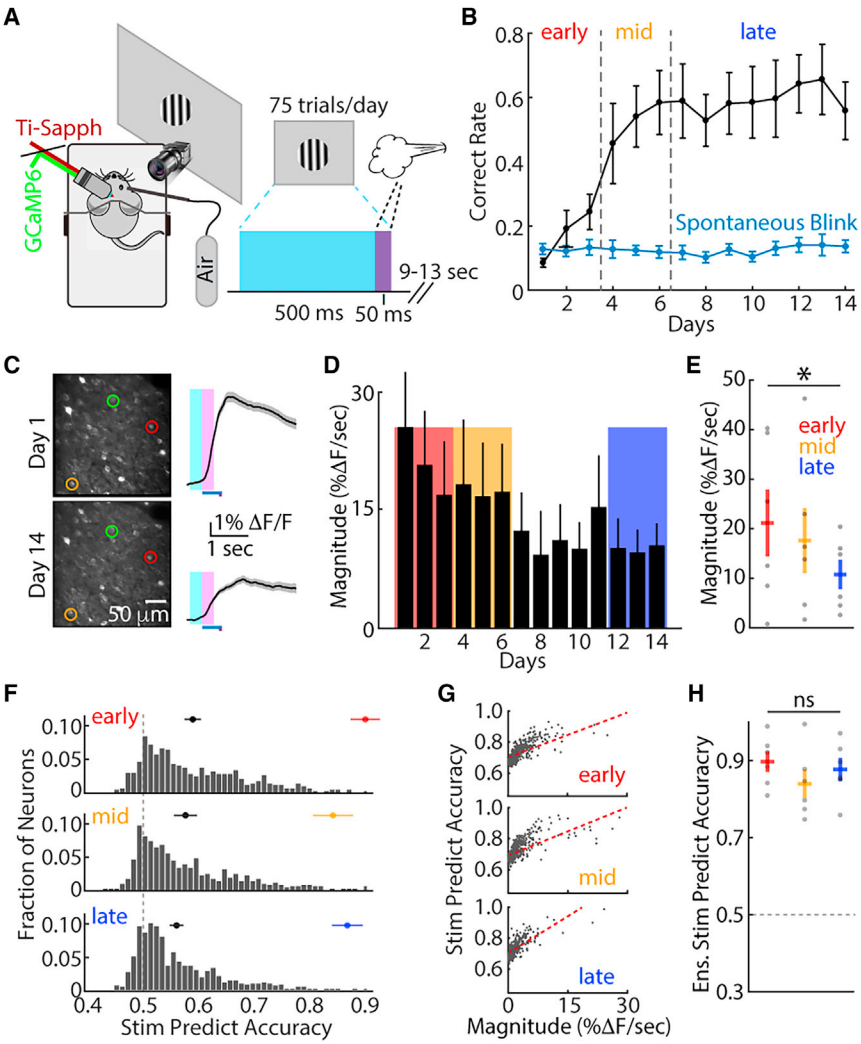

Figure 1. Longitudinal Imaging of Activity during Visually Cued Eyeblink Conditioning

(A) Schematic illustration of the behavioral setup (left) and trial structure (right).

(B) Performance over 14-day-long training for the layer 2/3 PN imaging cohort (n = 6 mice, black). Dots with error bars represent averages ± SEM. Spontaneous blink rate per 450 ms period is shown (blue). Training phases were divided into tertiles (early, mid, and late) based on average group performance.

(C) Example of *in vivo* two-photon imaging of layer 2/3 neurons expressing GCaMP6s, collected on two different training days from the same mouse. Scale bar indicates 50 μm. Average visually evoked response for one example layer 2/3 neuron on days 1 and 14 is shown to the right. Timing of the visual stimulus (blue bar) and air puff (purple bar) are shown below each trace. Intervals for measuring baseline activity (light-blue window) and visual response magnitude (pink window) are shown superimposed. Lines and shading indicate averages ± SEM across all trials for the given day.

(D) Population values for the visual response magnitude (given as %ΔF/s) for each day of training. Bars and lines indicate averages ± SEM. Analysis windows (3 days) for early (red), mid (orange), and late (blue) training phases are indicated.

(E) Average population values for response magnitude within each training phase, corresponding to colors in (D). Lines represent averages ± SEM (n = 6 mice). *p < 0.05, paired t test for early versus late.

(F) Distribution of stimulus prediction accuracy values using a linear decoder for responses of individual layer 2/3 neurons across each training phase. Chance level (0.5) is indicated (gray dashed line). Black circles indicate averages ± SEM for the population of individual neurons.

(G) Relationship between stimulus prediction accuracy and response magnitude for individual neurons across each training phase. Red dashed line indicates Spearman's rank correlation.

(H) Average stimulus prediction accuracy values using a linear decoder for the ensemble activity. Colors as in (D). Lines represent averages ± SEM (n = 6 mice) and are also indicated by colored circles in (F). *p < 0.05, t test relative to chance. ns indicates p > 0.05, paired t test for early versus late.

eyeblink conditioning task. Briefly, head-fixed mice placed on a running wheel learned to associate a contrast-modulated drifting grating (conditioned stimulus [CS]) with an aversive ipsilateral corneal air puff (unconditioned stimulus [US]), which elicited an unconditioned blink response (UR). Repeated stimulus pairings resulted in a conditioned blink response (CR), which occurred after the onset of the visual stimulus but before the air puff (Figure 1A; see Method Details). Learning occurred over a few days without change in CR magnitude or latency (Figures 1B and S1), and we previously showed that both acquisition and performance required an intact V1 (Tang and Higley, 2020). For subsequent analyses, learning was divided into three phases (early, mid, and late) based on average group performance (Figure 1B). Performance was only modestly dependent on behavioral state during the early learning phase, measured via either locomotion speed or pupil diameter, and the distribution of behavioral state parameters did not change across learning (Figure S1; Table S1; see Method Details).

We used two-photon imaging of the genetically encoded calcium indicator GCaMP6s (Chen et al., 2013b) to monitor the activity of putative pyramidal neurons (PNs) in V1 (see Method Details), tracking the same cells longitudinally across the 2-week training period (Figures 1C and S2). As we showed previously (Tang and Higley, 2020), spontaneous blinks can evoke responses in V1 neurons (Figure S2). To exclude any potential contamination of the measurements of stimulus-evoked responses, we restricted our analyses to a 300-ms period after stimulus onset, using the calculated linear slope (%ΔF/s) as the measure of response magnitude (Figure S2). Consistent with recent work (Makino and Komiyama, 2015), acquisition of visual behavior was associated with a reduction in the evoked response over the course of training (Figures 1C and 1D). This result was significant when directly comparing responses between early and late learning phases (21.1 ± 6.8% versus 10.8 ± 3.0%, n = 6 mice, paired t test, p = 0.028; Figure 1E; see Method Details). Control experiments revealed that visual

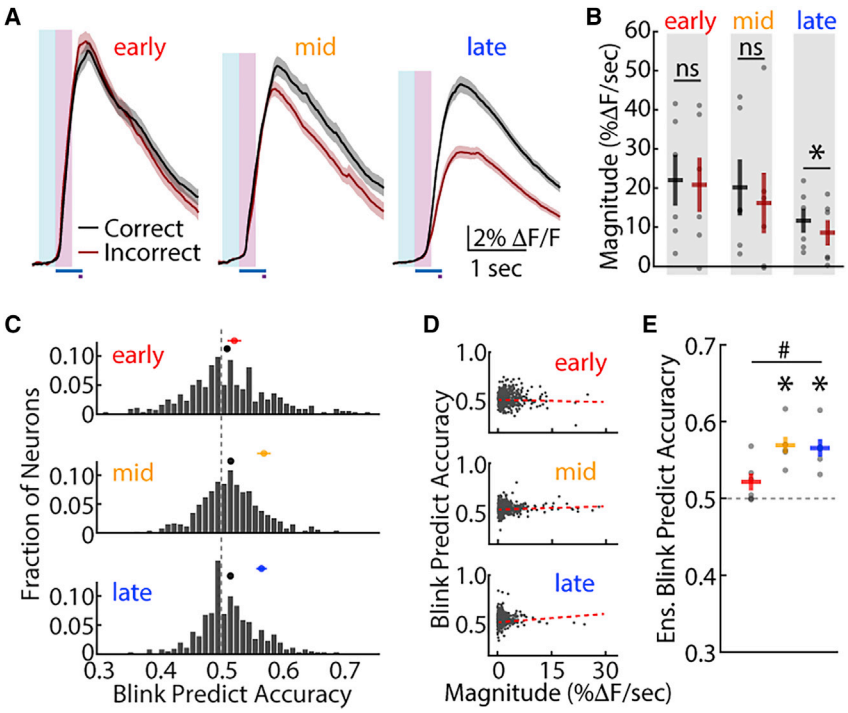

Figure 2. Cortical Representation of Behavioral Outcome Emerges during Training

(A) Average visually evoked response for one example layer 2/3 neuron across training phases. Traces are separated by correct (black) and incorrect (dark red) trials. Timing of visual stimulus (blue bar) and air puff (purple bar), and analysis windows (baseline, light blue; visual response, pink) are shown. Lines and shading indicate averages ± SEM across all trials for the given phase.

(B) Average population values for the visual response magnitude, separated by correct and incorrect trials, within each training phase. Lines represent averages ± SEM (n = 6 mice). *p < 0.05; ns indicates p > 0.05, paired t test for correct versus incorrect.

(C) Distribution of blink prediction accuracy values using a linear decoder for responses of individual layer 2/3 neurons across each training phase. Chance level (0.5) is indicated (gray dashed line). Black circles indicate averages ± SEM for the population of individual neurons.

(D) Relationship between blink prediction accuracy and response magnitude for individual neurons across each training phase. Red dashed line indicates Spearman's rank correlation.

(E) Average blink prediction accuracy values using a linear decoder for the ensemble activity. Colors denote training phases as above. Lines represent averages ± SEM (n = 6 mice) and are also indicated by colored circles in (C). *p < 0.05, t test relative to chance for each phase. #p < 0.05, paired t test for early versus late.

experience alone, in the absence of training, is sufficient to induce a reduction in sensory-evoked cortical activity (Figure S3; Table S1). Visual responses were enhanced by arousal (Vinck et al., 2015), although that modulation did not change across learning (Figure S3; Table S1). Interestingly, thalamic axons imaged in layer 4 exhibited a non-significant increase in response magnitude (Figure S3; Table S1), arguing that the experience-dependent decrease in V1 responses arises through modification of intracortical circuits.

To examine whether our observed changes in response magnitude were associated with disruption of stimulus encoding, we investigated the ability of a linear classifier to predict the presence of a visual stimulus versus baseline spontaneous activity for individual trials (see Method Details). Using a support vector machine (SVM) model, we found that individual PNs exhibited a range of stimulus prediction accuracy levels that did not differ across learning (early versus late phase, 0.59 ± 0.02 versus 0.56 ± 0.01, n = 6 mice, paired t test, p = 0.999; Kolmogorov-Smirnoff [KS] test, p = 0.956; Figure 1F). Interestingly, the stimulus-predictive accuracy of single neurons was correlated with response magnitude within a single learning phase (early: Spearman's r^2 = 0.52, p < 0.001; mid: Spearman's r^2 = 0.50, p < 0.001; late: Spearman's r^2 = 0.46, p < 0.001; Figure 1G). Previous work has shown that neuronal populations can perform much better than individual cells in predicting sensory stimuli (Moreno-Bote et al., 2014). Therefore, we trained a similar SVM using an ensemble vector comprising all neurons, confirming that, as a group, layer 2/3 PNs performed better than chance during all learning phases (early: 0.90 ± 0.03, n = 6 mice, t test, p < 0.001; mid: 0.84 ± 0.04, n = 6 mice, t test, p < 0.001; late: 0.88 ± 0.03, n = 6 mice, t test, p < 0.001; Figure 1H). In addition, population accuracy was unchanged over learning, despite the reduced response magnitude (early versus late, n = 6 mice, paired t test, p = 0.772; Figure 1H). Overall, these findings demonstrate that functional plasticity of evoked V1 response magnitude can occur without significant alteration in the ability to robustly encode sensory input.

Next, we examined whether visually evoked activity in V1 was predictive of an animal's behavioral performance. During early and mid-learning, there was no difference between the average PN response magnitude for correct versus incorrect trials (early: 22.0 ± 6.5% versus 20.8 ± 6.9%, n = 6 mice, paired t test, p = 0.188; mid: 20.2 ± 7.1% versus 16.2 ± 7.7%, n = 6 mice, paired t test, p = 0.235). However, in well-trained animals (late phase), responses on correct trials were larger than those on incorrect (11.7 ± 3.1% versus 8.6 ± 3.2%, n = 6 mice, paired t test, p = 0.003, Figures 2A and 2B). We again used a linear classifier to investigate neuronal predictive accuracy for trial outcome. Interestingly, the average accuracy of individual neurons increased over the 2-week training period (early versus late phase, 0.51 ± 0.004 versus 0.52 ± 0.003, n = 6 mice, paired t test, p = 0.039; KS test, p < 0.001; Figure 2C) and was not correlated with response magnitude (early: Spearman's r^2 < 0.001, p = 0.228; mid: Spearman's r^2 = 0.007, p = 0.082; late: Spearman's r^2 = 0.020, p = 0.086; Figure 2D). Consistent with the average response data, layer 2/3 PN ensembles were also not better than chance at predicting behavior during the early phase of training (0.52 ± 0.01, n = 6 mice, t test, p = 0.053) but did perform

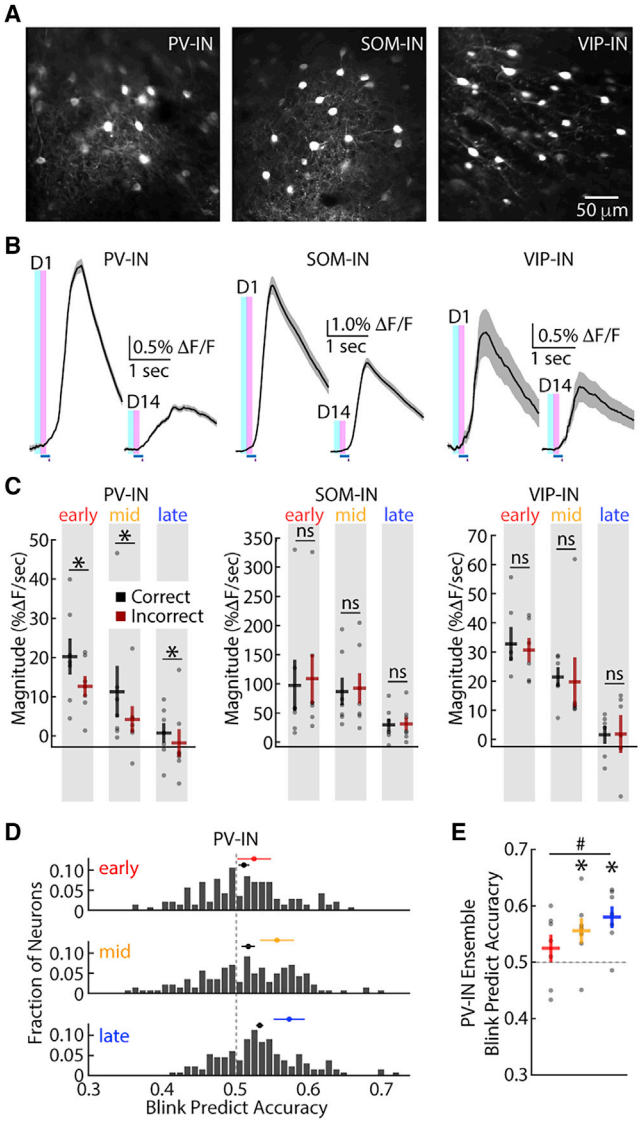

Figure 3. Sensory and Behavioral Representation by GABAergic Interneurons

(A) Example of *in vivo* 2-photon imaging of the GCaMP6f in layer 2/3 PV-INs (left), SOM-INs (middle), and VIP-INs (right). Scale bar indicates 50 μm.

(B) Average visually evoked responses for example layer 2/3 PV-INs (left), SOM-INs (middle), and VIP-INs (right). Traces are shown for days 1 and 14. Timing of visual stimulus (blue bar) and air puff (purple bar) and the analysis windows (baseline, light blue; visual response, pink) are shown. Lines and shading indicate averages ± SEM across all trials.

(C) Average population values for the visual response magnitude, separated by correct (black) and incorrect (dark red) trials, within each training phase. Data are for PV-INs (left), SOM-INs (middle), and VIP-INs (right). Lines represent averages ± SEM (PV-INs, n = 7 mice; SOM-INs, n = 7 mice; VIP-INs, n = 6 mice). *p < 0.05, paired t test for correct versus incorrect.

(D) Distribution of blink prediction accuracy values using a linear decoder for responses of individual layer 2/3 PV-INs across each training phase. Chance level (0.5) is indicated (gray dashed line). Black circles indicate averages ± SEM for the population of individual neurons.

(E) Average blink prediction accuracy values using a linear decoder for the ensemble activity of PV-INs. Lines represent averages ± SEM (n = 7 mice) and are also indicated by colored circles in (D). *p < 0.05, t test relative to chance for each phase. #p < 0.05, paired t test for early versus late.

better than chance for later phases (mid: 0.57 ± 0.01, n = 7 mice, t test, p < 0.001; late: 0.57 ± 0.01, n = 6 mice, t test, p < 0.001; Figure 2E), and the blink prediction accuracy was better for the late versus early phase (paired t test, p = 0.017). Furthermore, as with our behavioral data, performance prediction accuracy was not correlated with the sensitivity of individual neurons to changes in behavioral state (Figure S3; Table S1).

We next estimated the number of single cells necessary to reach population-level accuracy by training our classifier on randomly selected neuronal groups of varying size, finding that ~30 cells were sufficient to match the accuracy of the overall population (Figure S4). Simulating a population of neurons whose accuracy values matched the distribution of the layer 2/3 PNs confirmed that ensembles of ~30 cells exhibit markedly better predictive performance than the average of single cells and a corresponding improvement with the learning phase (early versus late, 0.47 ± 0.01 versus 0.95 ± 0.02, n = 80 synthetic neurons, t test, p < 0.001; Figure S4; Table S1). Thus, our results demonstrate the remarkable finding that the accurate representation of behavior in V1 is highly plastic, emerging during learning despite the unchanged accuracy of the stimulus prediction. Moreover, improved ensemble accuracy follows from the increasing accuracy of individual neurons through pooling of a relatively small number of cells.

To determine whether our findings generalized across all neuronal populations in V1, we again used two-photon imaging to monitor the activity of GABAergic INs expressing either PV, SOM, or VIP in separate cohorts of mice undergoing behavioral training (Figures 3A and S5). All three IN populations exhibited a reduction in stimulus-evoked response magnitude over the course of training, similar to the results from PNs (Figures 3B and S5; Table S1). As above, this change did not alter the ability of PV-, SOM-, or VIP-IN ensembles to accurately and stably predict the visual stimulus throughout training (Figure S5; Table S1). However, only the PV-INs demonstrated a difference between average response magnitude on correct versus incorrect trials (early: 20.1 ± 4.5% versus 12.6 ± 2.4%, n = 7 mice, paired t test, p = 0.031; mid: 11.1 ± 6.6% versus 4.2 ± 3.3%, n = 7 mice, paired t test, p = 0.047; late: 1.2 ± 2.1% versus −3.9 ± 2.1%, n = 7 mice, paired t test, p = 0.021; Figure 3C). Moreover, the linear classifier revealed that prediction accuracy of individual PV-INs for trial outcome increased with training (early versus late, 0.51 ± 0.01 versus 0.53 ± 0.004, n = 7 mice, paired t test, p = 0.013; KS test, p = 0.004; Figure 3D). Similarly, the behavioral prediction accuracy of PV-IN ensembles did not differ from chance during early training (0.52 ± 0.02, n = 7 mice, t test, p = 0.172) but did perform above chance for mid (0.56 ± 0.02, n = 7 mice, t test, p = 0.023) and late (0.58 ± 0.02, n = 7 mice, t test, p = 0.003; Figure 3E) phases, and there was an increase in accuracy between early and late training (paired t test, p = 0.021). Similar analyses for SOM- and VIP-INs revealed that behavioral prediction accuracy did not differ from chance at

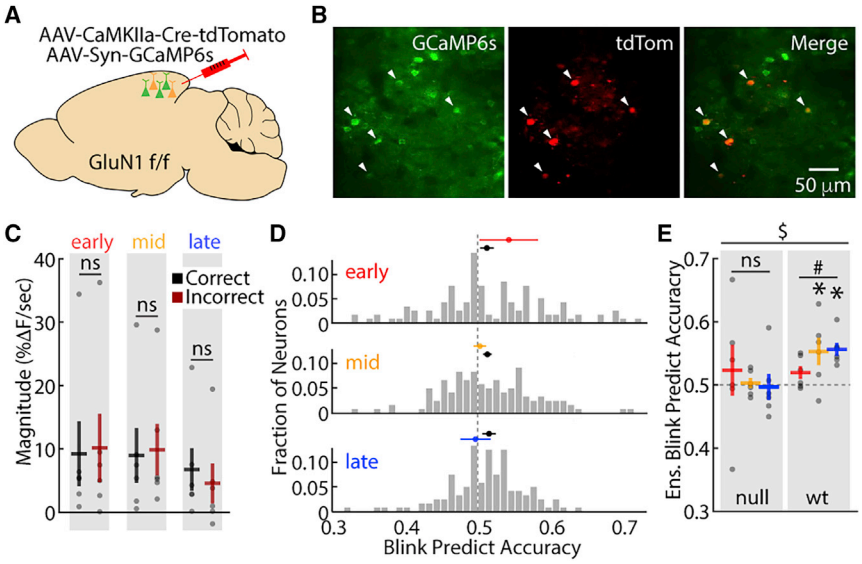

Figure 4. NMDARs Are Required for Functional Plasticity of Behavioral Representation

(A) Schematic illustration showing viral strategy for sparse deletion of the GluN1 subunit and expression of GCaMP6s.

(B) Example of *in vivo* two-photon image of GCaMP6s (green, left), tdTomato (red, middle), and merge (right) in layer 2/3 neurons. tdTomato-expressing cells are putative GluN1 null. Scale bar indicates 50 μm.

(C) Average population values for the visual response magnitude of GluN1 null cells, separated by correct (black) and incorrect (dark red) trials, within each training phase. Lines represent averages ± SEM (n = 6 mice). ns indicates $p > 0.05$, paired t test for correct versus incorrect.

(D) Distribution of blink prediction accuracy values using a linear decoder for responses of individual GluN1-null cells across each training phase. Chance level (0.5) is indicated (gray dashed line). Black circles indicate averages ± SEM for the population of individual neurons.

(E) Average blink prediction accuracy values using a linear decoder for the ensemble activity of GluN1-null and GluN1-WT cells. Lines represent averages ± SEM (n = 6 mice) and are also indicated by colored circles in (D). *$p < 0.05$, t test relative to chance for each phase; $^{\#}p < 0.05$ and ns indicates $p > 0.05$, respectively for early versus late; $^{\$}p < 0.05$, t test for late phase null versus WT.

any phase of training (Figure S5; Table S1). Overall, these data reveal that the emergence of behavioral representations during visual conditioning is specific to PNs and PV-INs.

The functional plasticity of the V1 activity associated with training might arise from modification of synaptic connectivity within local networks. NMDARs are strongly linked to synaptic plasticity of both excitatory and inhibitory synapses and may be necessary for experience-dependent changes in visually evoked responses (Chiu et al., 2018, 2019; Cooke and Bear, 2010; Frenkel et al., 2006; Malenka and Bear, 2004). To determine whether our results are dependent on NMDAR signaling, we used an adeno-associated virus (AAV) vector to delete the obligatory GluN1 subunit from a sparse number of V1 neurons (Chiu et al., 2018). Here, expression of Cre recombinase-tdTomato in GluN1f/f mice allowed us to identify the small number of putative GluN1 null cells (20.8 ± 3.0) in each field of view during imaging (Figures 4A and 4B). Sparse loss of NMDARs did not disrupt visual learning, and there was no difference in evoked-response magnitude between GluN1 null (tdTomato-positive) and neighboring wild-type (WT; tdTomato-negative) neurons (Table S1). Training the linear classifier on GluN1-null ensemble data showed that those cells accurately predicted the visual stimulus for all phases (Figure S6; Table S1). However, GluN1-null cells failed to develop a difference in average response magnitude for correct versus incorrect trials (early: 9.3 ± 5.1% versus 10.2 ± 5.4%, n = 6 mice, paired t test, $p = 0.703$; mid: 9.0 ± 4.2% versus 9.9 ± 4.2%, n = 6 mice, paired t test, $p = 0.686$; late: 6.6 ± 3.3% versus 4.5 ± 3.0%, n = 6 mice, paired t test, $p = 0.073$; Figure 4C). Consistent with that finding, the average blink prediction accuracy of single GluN1-null neurons did not improve with learning (early versus late, 0.51 ± 0.01 versus 0.52 ± 0.01, n = 6 mice, paired t test, $p = 0.386$; KS test, $p = 0.155$; Figure 4D). Additionally, the GluN1-null ensemble could not predict behavior above chance for any phase (early: 0.52 ± 0.04, n = 6 mice, t test, $p = 0.294$; mid: 0.50 ± 0.01, n = 6 mice, t test, $p = 0.362$; late: 0.50 ± 0.02, n = 6 mice, t test, $p = 0.557$), and accuracy did not improve over training (early versus late, paired t test, $p = 0.694$; Figure 4E). Importantly, we trained our classifier on a similarly sized (n = 20) population of randomly selected GluN1-WT neurons from the same fields of view. As with cells from WT mice, GluN1-WT neurons accurately predicted the visual stimulus for each phase, and that accuracy did not change across learning or differ between GluN1-null and -WT cells (Figure S6; Table S1). In addition, the GluN1-WT ensemble could not predict behavior during the early phase (0.52 ± 0.01, n = 6 mice, t test, $p = 0.055$) but performed better than chance for mid (0.55 ± 0.02, n = 7 mice, t test, $p = 0.029$) and late (0.56 ± 0.01, n = 6 mice, t test, $p = 0.001$) phases and demonstrated improvement with training (early versus late, paired t test, $p = 0.026$; Figure 4E). Moreover, in well-trained animals (late phase) the GluN1-WT cells predicted performance significantly better than the GluN1-null cells (t test, $p = 0.026$; Figure 4E).

DISCUSSION

Our results indicate that sensory-evoked neuronal activity in V1 is highly plastic during visual learning. Consistent with earlier work, response magnitude for both excitatory and inhibitory cells decreased over several days (Makino and Komiyama, 2015), although this decrease occurred without loss of predictive accuracy for the sensory stimulus. In addition, our data indicate that this reduced responsiveness also occurs in the absence of aversive stimuli, suggesting passive habituation is the default outcome, in contrast to earlier

findings (Gavornik and Bear, 2014). Notably, those changes in activity and prediction accuracy were not correlated with changes in behavioral state or arousal levels across learning. Previous studies have also shown that experience-dependent plasticity can alter the feature selectivity of V1 neurons (Gavornik and Bear, 2014; Goltstein et al., 2013; Jurjut et al., 2017; Makino and Komiyama, 2015; Poort et al., 2015; Schoups et al., 2001), whereas our data highlight the emergence of behavioral outcome representations early in the visual pathway. This finding builds on work from our laboratory and others demonstrating the ability of sensory areas to accurately encode behavioral choice (Chen et al., 2013a; Kwon et al., 2016; Poort et al., 2015; Tang and Higley, 2020) and indicates that this information is not inherent to V1 but develops during learning.

We observed an emergence of behavioral predictions in both PNs and PV-INs, but not in SOM- or VIP-INs, likely reflecting cell-type specificity of underlying plasticity mechanisms. This finding contrasts somewhat with earlier work demonstrating plasticity of stimulus tuning for PV- and SOM-INs during learning (Khan et al., 2018). PV-IN activity is closely linked to that of local excitatory networks and has a key role in regulating the timing and gain of sensory-evoked responses (Atallah et al., 2012; Cardin et al., 2009; Lee et al., 2012), making the functional coupling of these populations unsurprising. The presence of predictive accuracy for PV-INs even in early training likely reflects the difficulty in analyzing the earliest stages of learning given the small number of trials but suggests these cells rapidly gain this ability and may drive subsequent encoding by PNs. SOM-INs are linked to the control of dendritic calcium signaling and experience-dependent circuit plasticity (Chiu et al., 2013, 2018; Cichon and Gan, 2015; Hayama et al., 2013; Makino and Komiyama, 2015), suggesting that these cells may still contribute to the functional reorganization of V1 activity despite their lack of predictive accuracy. Notably, our previous work also demonstrated significant heterogeneity across PN subpopulations for both sensory and behavioral representations (Lur et al., 2016; Tang and Higley, 2020), further supporting the existence of functionally diverse but physically intermingled circuits in V1.

We also found that GluN1 deletion cell-autonomously abolished the plasticity of both response magnitude and behavioral representation, which indicates that the experience-dependent response difference on correct and incorrect responses does not simply reflect a change in the downstream correlation of V1 activity and motor output. Instead, intracortical NMDAR-dependent plasticity appears to be a fundamental contributor to the learning process. A large body of work supports a role for NMDARs in both excitatory and inhibitory synaptic plasticity (Chiu et al., 2019; Malenka and Bear, 2004), and future studies are necessary to examine whether modification of inputs to V1 PNs drives the functional circuit reorganization observed here.

Despite our findings that V1 is necessary for learning and performance of eyeblink conditioning and accurately encodes behavior, the association between CS and US is most likely driven by synaptic plasticity in the cerebellum (Freeman and Steinmetz, 2011), with the cortex providing a necessary throughput for visual information to reach the brainstem via pontine relays (Tang and Higley, 2020). We hypothesize that during learning, plasticity within V1 circuits refines their ability to gate this information flow, allowing behavior to be influenced by the broader behavioral context. Overall, our results indicate that excitatory and inhibitory V1 networks can multiplex stable representations of visual stimuli and dynamic representations of behavioral output. This work provides evidence that sensory and motor signals are inextricably linked, even within early sensory areas, to support the generation of complex behaviors.

STAR★METHODS

Detailed methods are provided in the online version of this paper and include the following:

- KEY RESOURCES TABLE
- RESOURCE AVAILABILITY
  - Lead Contact
  - Materials Availability
  - Data and Code Availability
- EXPERIMENTAL MODEL AND SUBJECT DETAILS
- METHOD DETAILS
  - Surgery
  - Behavioral Setup
  - Behavioral Training
  - Calcium Imaging
- QUANTIFICATION AND STATISTICAL ANALYSIS
  - Behavioral analysis
  - Imaging analysis and statistics

SUPPLEMENTAL INFORMATION

Supplemental Information can be found online at https://doi.org/10.1016/j.celrep.2020.107970.

ACKNOWLEDGMENTS

The authors are thankful to Dr. Lan Tang for initial design of the eyeblink-conditioning task and helpful comments during analyses. We also wish to thank Dr. Jessica A. Cardin as well as Mr. Daniel Barson, Dr. Tom Morse, and Dr. Garrett Neske and other members of the Higley Laboratory for helpful comments during the preparation of this manuscript. We thank Douglas Kim and the GENIE Project for the GCaMP6 and GCaMP7 plasmids. This work was supported by funding from the NIH/NIMH (R01 MH099045 and R01 MH113852 to M.J.H. and P30 EY026878 to the Yale Vision Core), the Yale Kavli Institute for Neuroscience (M.J.H.), and a Yale University Brown-Coxe postdoctoral fellowship (A.P.).

AUTHOR CONTRIBUTIONS

Experiments were conceived and designed by A.P. and M.J.H. Data were acquired by A.P. Analyses and interpretation were designed and carried out by A.P., H.B., and M.J.H. Manuscript was written by A.P. and M.J.H.

DECLARATION OF INTERESTS

The authors declare no competing interests.

CellPress
OPEN ACCESS

Received: November 20, 2019
Revised: January 28, 2020
Accepted: July 8, 2020
Published: July 28, 2020

REFERENCES

Albergaria, C., Silva, N.T., Pritchett, D.L., and Carey, M.R. (2018). Locomotor activity modulates associative learning in mouse cerebellum. Nat. Neurosci. *21*, 725–735.

Atallah, B.V., Bruns, W., Carandini, M., and Scanziani, M. (2012). Parvalbumin-expressing interneurons linearly transform cortical responses to visual stimuli. Neuron *73*, 159–170.

Blake, D.T., Heiser, M.A., Caywood, M., and Merzenich, M.M. (2006). Experience-dependent adult cortical plasticity requires cognitive association between sensation and reward. Neuron *52*, 371–381.

Cardin, J.A., Carlén, M., Meletis, K., Knoblich, U., Zhang, F., Deisseroth, K., Tsai, L.H., and Moore, C.I. (2009). Driving fast-spiking cells induces gamma rhythm and controls sensory responses. Nature *459*, 663–667.

Chen, J.L., Carta, S., Soldado-Magraner, J., Schneider, B.L., and Helmchen, F. (2013a). Behaviour-dependent recruitment of long-range projection neurons in somatosensory cortex. Nature *499*, 336–340.

Chen, T.W., Wardill, T.J., Sun, Y., Pulver, S.R., Renninger, S.L., Baohan, A., Schreiter, E.R., Kerr, R.A., Orger, M.B., Jayaraman, V., et al. (2013b). Ultrasensitive fluorescent proteins for imaging neuronal activity. Nature *499*, 295–300.

Chiu, C.Q., Lur, G., Morse, T.M., Carnevale, N.T., Ellis-Davies, G.C., and Higley, M.J. (2013). Compartmentalization of GABAergic inhibition by dendritic spines. Science *340*, 759–762.

Chiu, C.Q., Martenson, J.S., Yamazaki, M., Natsume, R., Sakimura, K., Tomita, S., Tavalin, S.J., and Higley, M.J. (2018). Input-specific NMDAR-dependent potentiation of dendritic GABAergic inhibition. Neuron *97*, 368–377.e363.

Chiu, C.Q., Barberis, A., and Higley, M.J. (2019). Preserving the balance: diverse forms of long-term GABAergic synaptic plasticity. Nat. Rev. Neurosci. *20*, 272–281.

Cichon, J., and Gan, W.B. (2015). Branch-specific dendritic Ca^{2+} spikes cause persistent synaptic plasticity. Nature *520*, 180–185.

Cooke, S.F., and Bear, M.F. (2010). Visual experience induces long-term potentiation in the primary visual cortex. J. Neurosci. *30*, 16304–16313.

Dana, H., Mohar, B., Sun, Y., Narayan, S., Gordus, A., Hasseman, J.P., Tsegaye, G., Holt, G.T., Hu, A., Walpita, D., et al. (2016). Sensitive red protein calcium indicators for imaging neural activity. Elife *5*, e12727.

Dubbs, A., Guevara, J., and Yuste, R. (2016). moco: fast motion correction for calcium imaging. Front. Neuroinform. *10*, 6.

Freeman, J.H., and Steinmetz, A.B. (2011). Neural circuitry and plasticity mechanisms underlying delay eyeblink conditioning. Learn. Mem. *18*, 666–677.

Frenkel, M.Y., Sawtell, N.B., Diogo, A.C., Yoon, B., Neve, R.L., and Bear, M.F. (2006). Instructive effect of visual experience in mouse visual cortex. Neuron *51*, 339–349.

Gavornik, J.P., and Bear, M.F. (2014). Learned spatiotemporal sequence recognition and prediction in primary visual cortex. Nat. Neurosci. *17*, 732–737.

Goltstein, P.M., Coffey, E.B., Roelfsema, P.R., and Pennartz, C.M. (2013). In vivo two-photon Ca2+ imaging reveals selective reward effects on stimulus-specific assemblies in mouse visual cortex. J. Neurosci. *33*, 11540–11555.

Hayama, T., Noguchi, J., Watanabe, S., Takahashi, N., Hayashi-Takagi, A., Ellis-Davies, G.C., Matsuzaki, M., and Kasai, H. (2013). GABA promotes the competitive selection of dendritic spines by controlling local Ca2+ signaling. Nat. Neurosci. *16*, 1409–1416.

Heiney, S.A., Wohl, M.P., Chettih, S.N., Ruffolo, L.I., and Medina, J.F. (2014). Cerebellar-dependent expression of motor learning during eyeblink conditioning in head-fixed mice. J. Neurosci. *34*, 14845–14853.

Hippenmeyer, S., Vrieseling, E., Sigrist, M., Portmann, T., Laengle, C., Ladle, D.R., and Arber, S. (2005). A developmental switch in the response of DRG neurons to ETS transcription factor signaling. PLoS Biol. *3*, e159.

Jurjut, O., Georgieva, P., Busse, L., and Katzner, S. (2017). Learning enhances sensory processing in mouse V1 before improving behavior. J. Neurosci. *37*, 6460–6474.

Khan, A.G., Poort, J., Chadwick, A., Blot, A., Sahani, M., Mrsic-Flogel, T.D., and Hofer, S.B. (2018). Distinct learning-induced changes in stimulus selectivity and interactions of GABAergic interneuron classes in visual cortex. Nat. Neurosci. *21*, 851–859.

Kwon, S.E., Yang, H., Minamisawa, G., and O'Connor, D.H. (2016). Sensory and decision-related activity propagate in a cortical feedback loop during touch perception. Nat. Neurosci. *19*, 1243–1249.

Lee, S.H., Kwan, A.C., Zhang, S., Phoumthipphavong, V., Flannery, J.G., Masmanidis, S.C., Taniguchi, H., Huang, Z.J., Zhang, F., Boyden, E.S., et al. (2012). Activation of specific interneurons improves V1 feature selectivity and visual perception. Nature *488*, 379–383.

Li, Z., Yan, A., Guo, K., and Li, W. (2019). Fear-related signals in the primary visual cortex. Curr. Biol. *29*, 4078–4083.e4072.

Lur, G., Vinck, M.A., Tang, L., Cardin, J.A., and Higley, M.J. (2016). Projection-specific visual feature encoding by layer 5 cortical subnetworks. Cell Rep. *14*, 2538–2545.

Makino, H., and Komiyama, T. (2015). Learning enhances the relative impact of top-down processing in the visual cortex. Nat. Neurosci. *18*, 1116–1122.

Malenka, R.C., and Bear, M.F. (2004). LTP and LTD: an embarrassment of riches. Neuron *44*, 5–21.

Moreno-Bote, R., Beck, J., Kanitscheider, I., Pitkow, X., Latham, P., and Pouget, A. (2014). Information-limiting correlations. Nat. Neurosci. *17*, 1410–1417.

Poort, J., Khan, A.G., Pachitariu, M., Nemri, A., Orsolic, I., Krupic, J., Bauza, M., Sahani, M., Keller, G.B., Mrsic-Flogel, T.D., and Hofer, S.B. (2015). Learning enhances sensory and multiple non-sensory representations in primary visual cortex. Neuron *86*, 1478–1490.

Ress, D., and Heeger, D.J. (2003). Neuronal correlates of perception in early visual cortex. Nat. Neurosci. *6*, 414–420.

Rutkowski, R.G., and Weinberger, N.M. (2005). Encoding of learned importance of sound by magnitude of representational area in primary auditory cortex. Proc. Natl. Acad. Sci. USA *102*, 13664–13669.

Schoups, A., Vogels, R., Qian, N., and Orban, G. (2001). Practising orientation identification improves orientation coding in V1 neurons. Nature *412*, 549–553.

Shuler, M.G., and Bear, M.F. (2006). Reward timing in the primary visual cortex. Science *311*, 1606–1609.

Siegel, J.J., Taylor, W., Gray, R., Kalmbach, B., Zemelman, B.V., Desai, N.S., Johnston, D., and Chitwood, R.A. (2015). Trace eyeblink conditioning in mice is dependent upon the dorsal medial prefrontal cortex, cerebellum, and amygdala: behavioral characterization and functional circuitry. eNeuro *2*, ENEURO.0051-14.2015.

Tang, L., and Higley, M.J. (2020). Layer 5 circuits in V1 differentially control visuomotor behavior. Neuron *105*, 346–354.e345.

Taniguchi, H., He, M., Wu, P., Kim, S., Paik, R., Sugino, K., Kvitsiani, D., Fu, Y., Lu, J., Lin, Y., et al. (2011). A resource of Cre driver lines for genetic targeting of GABAergic neurons in cerebral cortex. Neuron *71*, 995–1013.

Tsien, J.Z., Chen, D.F., Gerber, D., Tom, C., Mercer, E.H., Anderson, D.J., Mayford, M., Kandel, E.R., and Tonegawa, S. (1996). Subregion-

and cell type-restricted gene knockout in mouse brain. Cell *87*, 1317–1326.

Vinck, M., Batista-Brito, R., Knoblich, U., and Cardin, J.A. (2015). Arousal and locomotion make distinct contributions to cortical activity patterns and visual encoding. Neuron *86*, 740–754.

Wang, Y., Wu, W., Zhang, X., Hu, X., Li, Y., Lou, S., Ma, X., An, X., Liu, H., Peng, J., et al. (2016). A mouse model of visual perceptual learning reveals alterations in neuronal coding and dendritic spine density in the visual cortex. Front. Behav. Neurosci. *10*, 42.

Wiest, M.C., Thomson, E., Pantoja, J., and Nicolelis, M.A. (2010). Changes in S1 neural responses during tactile discrimination learning. J. Neurophysiol. *104*, 300–312.

Yan, Y., Rasch, M.J., Chen, M., Xiang, X., Huang, M., Wu, S., and Li, W. (2014). Perceptual training continuously refines neuronal population codes in primary visual cortex. Nat. Neurosci. *17*, 1380–1387.

Yang, T., and Maunsell, J.H. (2004). The effect of perceptual learning on neuronal responses in monkey visual area V4. J. Neurosci. *24*, 1617–1626.

STAR★METHODS

KEY RESOURCES TABLE

REAGENT or RESOURCE	SOURCE	IDENTIFIER
Bacterial and Virus Strains		
AAV5-Syn-Flex-GCaMP6f-WPRE-SV40	Chen et al., 2013b	Addgene Cat#100845
AAV5-Syn-GCaMP6s-WPRE-SV40	Chen et al., 2013b	Addgene Cat#100843
AAV5-Syn-jGCaMP7b-WPRE-SV40	Dana et al., 2016	Addgene Cat#104489
AAV8-Ef1a-Cre-tdTomato	Baylor Vector Core	Baylor Vector Core "AAV8-Ef1a-Cre-tdTomato"
Experimental Models: Organisms/Strains		
c57 Bl/6 mice	Envigo	Catalog specified as "C57BL/6 inbred mice"
SST-Cre mice	Taniguchi et al., 2011	JAX 013044
VIP-Cre mice	Taniguchi et al., 2011	JAX 031628
PV-Cre	Hippenmeyer et al., 2005	JAX 008069
Conditional GluN1 mice	Tsien et al., 1996	JAX 005246
Software and Algorithms		
ImageJ Moco Algorithm	Dubbs et al., 2016	https://github.com/NTCColumbia/moco
MATLAB	The Mathworks	Version 2018a, Statistics and Machine Learning Toolbox, https://www.mathworks.com/products/statistics.html

RESOURCE AVAILABILITY

Lead Contact

Further information and requests for resources and reagents should be directed to and will be fulfilled by the Lead Contact, Dr. Michael J. Higley (m.higley@yale.edu).

Materials Availability

This study did not generate new unique reagents.

Data and Code Availability

The datasets and code supporting the current study have not been deposited in a public repository due to file size limitations, but are available from the corresponding author on reasonable request. All data are presented in the paper and supplementary materials. The datasets generated during the current study are available from the corresponding author on reasonable request.

EXPERIMENTAL MODEL AND SUBJECT DETAILS

Animals were handled in accordance with the Yale Institutional Animal Care and Use Committee and federal guidelines. C57BL/6 mice were purchased from Envigo. PV^{Cre}/ C57/BL6 (Jackson laboratory, RRID: IMSR_JAX:008069), SST^{Cre}/ C57/BL6 (Jackson laboratory, RRID: IMSR_JAX:013044), VIP^{Cre}/ C57/BL6 (Jackson laboratory, RRID: IMSR_JAX:031628) and $GluN1^{fl/fl}$ (Jackson laboratory, RRID: IMSR_JAX: 005246) mice were bred in-house from animals originally purchased from Jackson Laboratory (Hippenmeyer et al., 2005; Taniguchi et al., 2011; Tsien et al., 1996). Animals of both sexes were used and aged 8-10 weeks old at the beginning of the experimental procedures. All mice were group housed (2-3 same-sex animals per cage) under a 12 h/12 h light/dark cycle with water and food provided *ad libitum*. From the day of the first stereotaxic surgery, animals were fed sulfatrim mouse chow (Uniprim). All experiments were performed during the light phase of the daily cycle. In all housing and experimental rooms, the temperature was maintained at 23-24°C, with humidity levels between 35% and 45%.

METHOD DETAILS

Surgery

Five weeks prior to imaging and behavioral experiments, mice were injected stereotactically with an adenoassociated viral (AAV) vector driving expression of a genetically encoded calcium indicator either in non-specific neuron populations (AAV5-syn-GCamP6s, C57BL/6 mice), targeted populations of interneurons (AAV5-syn-flex-GCamp6f, PV^{Cre}/ C57/BL6, SST^{Cre}/ C57/BL6 or

VIP^{Cre}/ C57/BL6 mice), or thalamocortical axonal terminals arising from the lateral geniculate nucleus (AAV5-syn-jGCaMP7b, C57BL/6 mice) (Chen et al., 2013b; Dana et al., 2016). To examine the effects of deletion of the GluN1 subunit of the NMDA-type glutamate receptor, GluN1$^{fl/fl}$ animals were injected with AAV5-syn-GCamP6s and dilute AAV5-EF1a-iCre-TdTomato (Baylor Vector Core, 1:300 in saline). Mice were anesthetized with isoflurane and received subcutaneous injection of an analgesic and anti-inflammatory drug (Carprofen 2mg/ml in saline, 5ml/kg). Mice were then placed in a stereotaxic apparatus (David Kopf Instruments) and their scalp shaved and disinfected with 70% ethanol. Ocular lubricant was used to protect animals' eyes from drying during surgery. To deliver the viruses into the left visual cortex (V1, coordinates AP: −0.35 cm; LM: −0.25 cm; DV: −0.055 cm) and dorsal lateral geniculate nucleus (dLGN, coordinates AP: −0.235 cm; LM: −0.2 cm; DV: −0.29 cm), we used a Nanofil 36G beveled needle inserted through a small craniotomy. The syringe was connected to a Micro Syringe Pump (World Precision Instruments) used to deliver virus (0.5-0.7 μL or 0.2 μL of total volume for cortical or thalamic injections respectively, 100 nl/min). After the injection, the needle remained in the brain for 5 min to allow for diffusion of the virus. Seven to ten days after viral injections, animals were implanted with cranial windows and titanium head-posts. Subjects were anesthetized with isoflurane and received subcutaneous injection of an analgesic and anti-inflammatory drug (Carprofen 2mg/ml in saline, 5ml/kg). Skin and periosteum were reflected and the skull was cleaned with saline and dried. Two screws were set into the skull over the right hemisphere, and a custom-made titanium headpost (~2g) was fixed to the bone with dental cement (Metabond, Parkell). A craniotomy (approx. 4 mm^2) was made over the left V1 and a bilayer cranial window (5x5mm No. 1 cover glass and 3.5x3.5 No. 1 cover glass, bonded using ultraviolet-curing adhesive, Norland Products) was inserted into the opening and fixed to the skull using instant glue (Krazy Glue) and dental cement (Metabond, Parkell).

Behavioral Setup

The mouse was head-fixed on a freely-moving wheel (15 cm diameter) under the objective of a 2-photon microscope located in a light-proof chamber. Visual stimuli were displayed on a computer monitor positioned normal to and 22 cm away from the right eye. Air-puffs (10-12 psi) were delivered to the right cornea via a small metal cannula coupled to a compressed air tank and gated by a solenoid (Clark Solutions). Timing of the air puff was coordinated with the visual stimulus using custom-written MATLAB codes through a NI-DAQmx board (PCIe-6315, National Instruments) at a sampling rate of 5 kHz. Eyelid closure and pupil diameter were continuously recorded using a monochromatic CMOS camera (PointGrey FlyCapture3) at a frame rate of 33 fps. An infrared LED array was used to illuminate the eye. All signals, including the timing of the visual stimuli, the air puffs, the wheel position, video frame ticks, and microscope resonant scanner frame ticks were digitized (5 kHz) and collected through a Power 1401 (CED) acquisition board using Spike 2 software.

Behavioral Training

Starting nine days prior to training, mice were habituated to head-fixation while placed on a freely-moving running wheel (15 cm diameter), gradually increasing from a few minutes to one hour over this period. After habituation, training consisted of 75 daily presentations to the right eye of a 500 ms visual stimulus (CS+) presented on a gamma-corrected monitor (20° sinusoidally drifting grating, 0.05 cycles per degree, 1 cycle/sond, 100% contrast). For each animal, the stimulus location was fixed in one of nine 3x3 sub-regions of the screen that evoked the largest population response in the field of view. Each stimulus co-terminated with a 50 ms air-puff directed to the ipsilateral cornea. Training was carried out over 14 consecutive days (Days 1-14). In addition to this protocol, on the day preceding training (Day 0) and the day following training (Day 15), each animal was presented with 50 CS presentations in the absence of a coupled air-puff. For all training days, the inter-trial interval was 9-13 s, with each trial value randomly selected from a flat hazard distribution.

Calcium Imaging

Imaging was carried out using a two-photon Movable Objective Microscope (MOM) with a galvo-resonant scanner (Sutter Instruments) through a 25x, 1.05 NA objective (Olympus) coupled to a Ti-sapphire laser (MaiTai eHP DeepSee, SpectraPysics) tuned to 920 nm. Collection of tdTomato images were carried out at 1000 nm. Images were acquired using ScanImage 2017 (Vidrio) at ~30 Hz and a resolution of 256x256. The microscope and the perimeter of the objective were tightly wrapped in blackout material to prevent light contamination from the LCD screen. Somata of layer 2/3 neurons were imaged at approximately 180-300 μm depth relative to the brain surface (Lur et al., 2016). Thalamocortical axons in layer 4 were imaged at 330-460 μm depth. Chronic imaging of neurons did not alter cell health as measured by the spontaneous activity of single cells (Figure S1).

QUANTIFICATION AND STATISTICAL ANALYSIS

Details for all statistical analyses, including statistical tests used, exact value of n, what n represents, and precision measures (e.g., mean, SEM) are provided in the Results section and in Table S1.

Behavioral analysis

Eyeblink videos were analyzed with custom MATLAB scripts as previously described (Tang and Higley, 2020). Briefly, gray-scale images from each training session were binarized to maximize the contrast between the eye (white) and surrounding fur (black). A region of interest around the eye was manually defined, and the time-varying proportion of white to dark pixels was used as a readout of eye

closure. These data were normalized by the 5th and 95th percentile values for each session, resulting in a range of 0 to 1, corresponding to a fully open and fully closed eye, respectively. The conditioned response (CR) was defined as the maximum eye closure during the 450 ms window between visual stimulus and air-puff onset. The unconditioned response (UR) was defined as the maximum eye closure within a 500 ms window from the onset of the air-puff. Trials were identified as correct if the CR:UR ratio was larger than 0.1. Trials were excluded from analysis if the eye closed > 10% within a 2 s window prior to visual stimulus onset. Spontaneous blinks (> 10% eye closure) were detected during the inter-trial-intervals. The spontaneous blink rate was calculated as the average number of blinks per 450 ms interval to compare with the behavioral analysis window. Pupil size and locomotion (running speed) data were binarized using the median normalized value and a cutoff of 1 cm/sec, respectively.

Imaging analysis and statistics

Images of neuronal activity were first motion-corrected using the Moco plugin for ImageJ (Dubbs et al., 2016). The first 150 frames of each movie were used as a template with the maximal distance to be translated in the x and y directions between 20 and 40 pixels. Videos from successive days were translated onto the first-day template. Regions of interest (ROIs) were selected manually (Lur et al., 2016). Further data analysis was performed using custom MATLAB scripts. Fluorescence (F) over time was measured by averaging within the ROI, and contamination from the surrounding neuropil was removed with a discounting coefficient of 0.7 (Chen et al., 2013b). $\Delta F/F$ was calculated as $(F-F_0)/F_0$, where F_0 was the lowest 10% of values from the neuropil-subtracted trace for each session.

To relate neuronal activity to behavior, we divided the data into 3 distinct learning phases of equal duration based on average performance: early (days 1 to 3), mid (days 4 to 6), and late (days 12-14). All data were grouped within a single phase. The magnitude of the visual response on each trial was defined in one of two ways: (1) the mean $\Delta F/F$ in a 300ms time window after visual stimulus onset, subtracting the mean $\Delta F/F$ over the 300 ms preceding the stimulus or (2) the slope of the visual response measured as the linear fit to $\Delta F/F$ within 300ms window following visual stimulus onset. Preliminary analyses revealed that the two measures were strongly correlated with each other but the slope value yielded significantly lower variation across trials (Figure S1). Thus, slope was primarily used for subsequent analyses. Machine learning was used to decode neuronal activity and assess the accuracy of predicting either the visual stimulus or the conditioned response. A linear Support Vector Machine (SVM) classifier was trained and tested by using an available MATLAB toolkit, libsvm, with 5-fold cross-validation and bootstrapping to achieve balanced labels for correct versus incorrect trials. To determine prediction accuracy for the visual stimulus, for each trial we quantified the slope of $\Delta F/F$ for the 300ms preceding and following the visual stimulus onset. We also identified a similar matched pair of values obtained for a randomly selected pseudo-onset during the inter-stimulus period. The model was trained to classify the presence of a visual stimulus (i.e., distinguish trials from pseudo-trials). A similar approach was used to determine prediction accuracy for single cells and for the population. To determine prediction accuracy for the conditioned response, we used only paired slope values corresponding to actual stimulus onset times and trained the model to classify correct versus incorrect trials. Again, this approach was used to determine single cell and population performance. To determine how population size influences behavioral prediction accuracy, we repeatedly trained the model on randomly drawn neuronal subsets of varying size. To investigate the relationship between average single neuron performance and population performance, we simulated a distribution of 80 independent slope values for 75 trials, matching the means and variances of the actual neuronal data on correct and incorrect trials and across learning phases. We then used these simulated values to train the same SVM model and assess simulated accuracy.

For all statistical comparisons of neuronal data, values were averaged within each animal, and final analyses were performed with animal number as the degree of freedom. We opted for this approach given the inherent lack of independence for cells imaged within the same animal. The analysis of simulated neuronal performance was an exception to this approach, given the inherent structure of the data. Statistical tests included paired and one-sample t tests using an alpha value of 0.05, Kolmogorov-Smirnoff tests, and Spearman's rank correlation. Planned comparisons were explicitly carried out for early and late learning phases (mid-phase data shown only for completeness of data representation).